Propulsion and Power Research 2023;12(4):523−538

http://ppr.buaa.edu.cn/

Propulsion and Power Research

www.sciencedirect.com

ORIGINAL ARTICLE

Analytical analysis of inclined three-layered composite channel with cobalt ferrite nanoparticles and Hall current in Darcy medium

P.V. Ananth Subray[a], B.N. Hanumagowda[a], C.S.K. Raju[b], S.V.K. Varma[a], Prakash Jagdish[c], Se-Jin Yook[b,*], Nehad Ali Shah[d]

[a]*Department of Mathematics, School of Applied Sciences, REVA University, Bengaluru, Karnataka, India*
[b]*School of Mechanical Engineering, Hanyang University, 222 Wangsimni-ro, Seongdong-gu, Seoul 04763, Republic of Korea*
[c]*Department of Mechanical Engineering Science, Faculty of Engineering & The Built Environment, University of Johannesburg, South Africa*
[d]*Department of Mechanical Engineering, Sejong University, Seoul 05006, Republic of Korea*

Received 6 March 2023; accepted 8 October 2023
Available online 25 November 2023

KEYWORDS

Three-layered flow;
Inclined composite channel;
Electromagnetic field;
Nanofluid;
Porous region

Abstract The present study explores the influence of electromagnetic effects on the flow of a nanofluid in a saturated permeable medium, confined between a clear viscous fluid in an inclined channel. The nanofluid consists of cobalt ferrite nanoparticles dispersed in ethylene glycol. The governing equations are derived considering Darcy's law for the permeable medium and Tiwari's model for fluids containing nano-sized particles. Additionally, radiation and dissipation effects are incorporated into the energy equation. The equations are transformed into dimensionless form and solved analytically using the perturbation technique. The results are analyzed through graphs and tables for different material parameters. The findings reveal that higher electric and magnetic strengths have a significant impact on the fluid velocity at the interface of the two fluids, resulting in reduced shear both at the clear fluid surface and the interface between them. This highlights the crucial role played by electric and magnetic strengths in modifying flow phenomena. Consequently, combining electric and magnetic strengths with

*Corresponding author.
E-mail address: ysjnuri@hanyang.ac.kr (Se-Jin Yook).

Peer review under responsibility of Propulsion and Power Research.

Production and Hosting by Elsevier on behalf of KeAi

https://doi.org/10.1016/j.jppr.2023.11.001

nanofluids can be utilized to achieve desired qualities in multi-fluid flow and enhance heat transfer characteristics.

Nomenclature

ω	angle of inclination
br	brinkman number
Gr	thermal Grashof number
ϕ	solid volume fraction
σ	porous medium parameter
g	gravitational force (unit: $m \cdot s^{-1}$)
ρ	density of the fluid (unit: $kg \cdot m^{-3}$)
θ	dimensionless temperature
E	electric field
M	magnetic field
N	thermal radiation
Nu	Nusselt number
τ	skin friction
k	thermal conductivity (unit: $W \cdot m^{-1} \cdot K^{-1}$)
μ	dynamic viscosity (unit: $kg \cdot m^{-1} \cdot s^{-1}$)
v	kinematic viscosity (unit: $m^2 \cdot s^{-1}$)
β	thermal expansion coefficient (unit: K^{-1})
κ	porosity of the porous medium
w	condition at the surface

Subscripts

nf	nanofluid
f	base fluid
s	solid particle

1. Introduction

Cobalt ferrite ($CoFe_2O_4$) is a spinel ferrite and has fascinated many researchers from different backgrounds [1,2]. Cobalt ferrite nanoparticles (CFNPs) have relatively high coercive force, large magneto crystalline anisotropy and are chemically stable. The flow of CFNPs in immiscible regions in the presence of an electromagnetic field has applications in many technical processes such as nano-clusters [3], gas detectors [4], ferrofluids, magnetic data storage [5] and biomedical applications [6–8]. Heat transfer in a fluid can be enhanced by using nanosized particles because they increase thermal conductivity when a small number of nanoparticles are added [9,10].

The amount of heat transferred can be improved by considering the porous medium. The use of a permeable medium in channels and heat exchangers made of metals. Farahani et al. [11] investigated the impact of incorporating microchannel-porous media and nanofluid on the temperature and performance of a CPV (concentrated photovoltaic) system. The use of these technologies aims to enhance heat transfer and overall system efficiency. This study explores the flow and heat transfer of nanofluids in a porous medium, considering velocity slip and temperature jump effects. The investigation reveals the existence of multiple solutions, highlighting the complexity and diversity of nanofluid behaviour in porous media was studied by Usafzai et al. [12]. A critical review was carried out by Habibishandiz and Saghir on various methods for enhancing heat transfer in the presence of porous media, nanofluids, and microorganisms [13]. It evaluates the effectiveness and applicability of these techniques, shedding light on their potential for improving heat transfer performance in different applications. When the porous medium is equipped the surface area between the liquid and solid surface increases. Hence using both permeable medium and nano-sized particles can give rise to the higher efficiency of the system.

Drag force is the main reason for the fluid to flow in immiscible regions which are created due to the shear stress which is investigated by a few researchers. Hibara et al. [14] investigated the multilayer system of microchips used in electronic gadgets where the connecting medium of liquids. Khaled [15] examined heat transfer enhancement in a vertical tube with two immiscible falling co-flows. The aim is to understand the heat transfer characteristics and potential enhancements in such a configuration. This research provides valuable insights into optimizing heat transfer performance in vertical tube systems with multiple immiscible co-flows. Umavathi and Bég [16] carried out a numerical study examining the effects of thermophysical properties on heat transfer at the interface of two immiscible fluids in a vertical duct. The investigation focuses on understanding the influence of these properties on heat transfer mechanisms and performance in such systems. The entropy generation minimization analysis to evaluate and optimize heat transfer processes between two immiscible fluids was carried out by Chen and Jian [17]. The analysis aims to reduce the overall entropy generation, improving the efficiency and effectiveness of heat transfer in systems involving immiscible fluid interfaces.

Conducting and non-conducting fluids were investigated by Malashetty et al. [18] in two immiscible regions to examine the flow rate and temperature distribution. Chamkha [19] considered the two-phase flow of conducting fluid in the presence of a permeable medium and heat source/sink.

Sheikholeslami et al. [20] deliberated the effect of a magnetic field over a two-phase unsteady fluid flow to determine the strength of flow and heat transfer using the numerical technique. A similar study related to two-phase flow was carried out by Ananth et al. [21], Bég [22], Khaled [23] and Alzahrani [24].

The three-phase flow of micropolar fluid squeezed in among glutinous fluid was deliberated by Umavathi et al. [25], they considered the flow to be due to pressure. Also, Umavathi and Sheremet [26] investigated three immiscible region flows consisting of couple stress nanofluid which is bounded by clear fluids. They noted that an increase in a couple stress constraints increases temperature and fluid flow. Hasnain et al. [27] analyzed the heat flux in Cattaneo-Christov fluid in a saturated permeable medium. They found out that thermal conductivity can be enhanced by using Cu nanoparticles compared to other particles. Moses et al. [28] investigated the unsteady MHD three-phase flow assuming the superior and inferior channels to be non-porous. Umavathi et al. [29], Nikodijevic et al. [30], Rauf and Naz [31], Tanuja et al. [32], and Kumar [33] have conducted analogous studies on two-phase flow.

From the literature, no such work is done for the betterment of heat transfer rate in three immiscible fluid flows through a permeable medium bounded above and below by clear fluids and in the presence of thermal radiation and electromagnetic fields. Another novel aspect of this work is the consideration of the nanoparticles in the presence of an electromagnetic field which yields a high rate of heat transfer. The individuality of the current study is presented in Table 1, it is obtained from the above-mentioned literature review, which is crucial for optimizing production rates and maximizing resource recovery in petroleum industries, hence we wish to consider these effects on the flow in this study.

2. Model formulation

Ethylene glycol-based cobalt ferrite nanofluid is considered in this investigation whose properties are mentioned in Table 2.

In the study stable, laminar and convective three-phase flow over an inclined plane placed in a permeable medium under the influence of the magnetic field that form $\vec{B}(0, B_0, 0)$ an electric field $\vec{E}(0, 0, E_0)$. The wall $y = -1$ is

Table 1 Novelty of the present work.

	Umavathi [26]	Hasnain [27]	Moses [28]	Umavathi [34]	Present study
Three-phase flow	✓	✓	✓	✓	✓
Porous medium	✓	✓	✓	✓	✓
Nanofluid flow	✗	✓	✗	✓	✓
Magnetic field	✗	✗	✓	✓	✓
Electric field	✗	✗	✗	✗	✓
Thermal radiation	✗	✗	✗	✗	✓
Inclined channel	✗	✗	✗	✗	✓

Table 2 Thermo-physical properties at room temperature.

Thermo physical properties	Ethylene glycol ($C_2H_6O_2$) [38]	Cobalt ferrite (CoF_2O_4) [38]	CNTs [39]	Alumina (Al_2O_3) [39]	Silver
ρ (kg/m^3)	1.115	4907	2600	3970	10,500
C_p (J/(kg·K))	0.58	700	42.5	756	235
k (W/mK)	0.1490	3.7	6600	40	429
$\beta \times 10^{-5}$ (1/K)	6.5	2.1	2.5	0.85	1.89
σ (S/m)	1.07×10^{-6}	0.84×10^{6}	0.71×10^{6}	1.07×10^{-6}	6.30×10^{7}

kept at T_{w2} and $y = 2$ is maintained at T_{w1}. The channel is separated into three regions, two of which consist of clear fluid in the presence of viscous, Joules and Darcy dissipation (Region-1 & Region-3). The second region is of a porous medium and consists of nanoparticles. The current density is given by $J = \sigma[\vec{E} + \vec{u} \times \vec{B}]$. Both thermal conductivity and viscosity are variable only with temperature. Density throughout the flow is assumed to be constant, excluding when it is associated with gravity (Boussinesq approximation [35]). Pressure and buoyancy are the main reasons for fluid flow. The geometry of the three-phase flow is shown in Figure 1.

Under these assumptions, and adopting the nanofluid model proposed by Tiwari's model [36] and permeable medium in the form of Darcy's law [37], the momentum and energy equations can be written as follows (Mose [28], Nikodijevic [30] and Umavathi [34]).

In Region-1

$$\mu_f \frac{d^2u_1'}{dy'^2} + (\rho_f g \beta_f)(T_1 - T_{w2})\cos(\omega) - \frac{\partial p}{\partial x} - \sigma_f (E_0 + B_0 u_1) B_0 = 0 \tag{1}$$

$$k_f \frac{d^2T_1}{dy'^2} + \mu_f \left(\frac{du_1'}{dy'}\right)^2 - \frac{\partial q^*}{\partial y} + \sigma_f (E_0 + B_0 u_1)^2 = 0 \tag{2}$$

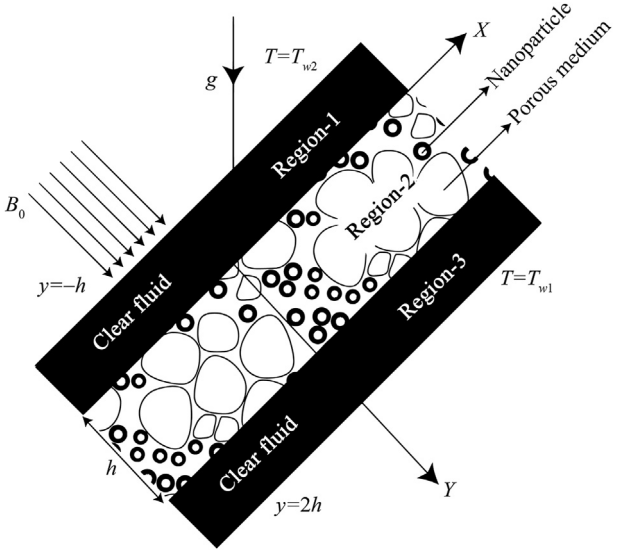

Figure 1 Geometry of the three-phase flow.

In Region-2

$$\mu_{nf} \frac{d^2u_2'}{dy'^2} + (\rho_{nf} g \beta_{nf})(T_2 - T_{w2})\cos(\omega) - \frac{\mu_{nf}}{\kappa} u_2' - \frac{\partial p}{\partial x} - \sigma_{enf} (E_0 + B_0 u_2) B_0 = 0 \tag{3}$$

$$k_{nf} \frac{d^2T_2}{dy'^2} + \mu_{nf} \left(\frac{du_2'}{dy'}\right)^2 + \frac{\mu_{nf}}{\kappa} u_2'^2 - \frac{\partial q^*}{\partial y} + \sigma_{enf} (E_0 + B_0 u_2)^2 = 0 \tag{4}$$

In Region-3

$$\mu_f \frac{d^2u_3'}{dy'^2} + (\rho_f g \beta_f)(T_3 - T_{w2})\cos(\omega) - \frac{\partial p}{\partial x} - \sigma_f (E_0 + B_0 u_3) B_0 = 0 \tag{5}$$

$$k_f \frac{d^2T_3}{dy'^2} + \mu_f \left(\frac{du_3'}{dy'}\right)^2 - \frac{\partial q^*}{\partial y} + \sigma_f (E_0 + B_0 u_3)^2 = 0 \tag{6}$$

Boundary and interface conditions are assumed to be (with reference to Umavathi [34]):

	Velocity	Temperature
at $y = -h$	$u_1'(y) = 0$	$T_1(y) = T_{w2}$
at $y = 0$	$u_1'(y) = u_2'(y)$	$T_1(y) = T_2(y)$
	$\mu_f \frac{du_1'(y)}{dy'} = \mu_{nf} \frac{du_2'(y)}{dy'}$	$k_f \frac{dT_1(0)}{dy'} = k_{nf} \frac{dT_2(0)}{dy'}$
at $y = h$	$u_2'(y) = u_3'(y)$	$T_2(y) = T_3(y)$
	$\mu_{nf} \frac{du_2'(y)}{dy'} = \mu_f \frac{du_3'(y)}{dy'}$	$k_{nf} \frac{dT_2(y)}{dy'} = k_f \frac{dT_3(y)}{dy'}$
at $y = 2h$	$u_3'(y) = 0$	$T_3(y) = T_{w1}$

(7)

Where μ_{nf} are modified viscosity and ρ_{nf} is the effective density of nanofluid, it is considered in the following form:

$$\mu_{nf} = \frac{\mu_f}{(1-\phi)^{2.5}}, \quad \rho_{nf} = (1-\phi)\rho_f + \phi\rho_s \tag{8}$$

The expression of other nanofluid parameters such as thermal diffusivity, heat capacitance and thermal expansion are considered as follows:

$$(\rho C_p)_{nf} = (1-\phi)(\rho C_p)_f + \phi(\rho C_p)_s$$

$$(\rho\beta)_{nf} = (1-\phi)(\rho\beta)_f + \phi(\rho\beta)_s,\ \alpha_{nf} = \frac{K_{nf}}{(\rho C_p)_{nf}} \tag{9}$$

$$(\rho\beta_c)_{nf} = (1-\phi)(\rho\beta_c)_f + \phi(\rho\beta_c)_s$$

According to Maxwell [40], the following equations represent the nanofluid's thermal conductivity:

$$K_{nf} = K_f\left\{\frac{K_s + 2K_f + \phi(K_f - K_s)}{K_s + 2K_f - 2\phi(K_f - K_s)}\right\} \tag{10}$$

To reduce Eqs. (1) to (7) to a dimensionless form we use:

$$y = \frac{y'}{h},\ u_i = u_i'\left(\frac{\rho_f}{\mu_f}\right)h,\ \theta_i = \frac{T_i - T_{w2}}{T_{w1} - T_{w2}},\ M^2 = \frac{B_0^2 h_1^2 \sigma}{\mu_f},$$

$$Gr = \frac{g\beta_f(T_{w1} - T_{w2})h^3}{\nu_f^2}\cos(\omega),\ E = \frac{E_0\rho_f h}{B_0\mu_f},\ \sigma = \frac{h}{\sqrt{\kappa}},$$

$$Br = \frac{\mu_f^3}{\rho_f^2 h^2 (T_{w1} - T_{w2})k_f},\ P = -\frac{\rho_f h^3}{\mu_f^2}\frac{\partial p}{\partial x},\ \nu_f = \frac{\mu_f}{\rho_f},$$

$$\frac{\partial q}{\partial y} = 4\alpha^2(T_i - T_{w2}),\ N = 2\alpha\frac{h}{\sqrt{k_f}}$$

a. Non-dimensionalized equations

In Region-1

$$\frac{d^2u_1}{dy^2} + Gr\theta_1 + P - M^2(E + u_1) = 0 \tag{11}$$

$$\frac{d^2\theta_1}{dy^2} + Br\left(\frac{du_1}{dy}\right)^2 - N^2\theta_1 + BrM^2(E + u_1)^2 = 0 \tag{12}$$

In Region-2

$$\frac{d^2u_2}{dy^2} + AGr\theta_2 - \sigma^2 u_2 + P_1 - B_1(E + u_2)M^2 = 0 \tag{13}$$

$$\frac{d^2\theta_2}{dy^2} + CBr\left\{\left(\frac{du_2}{dy}\right)^2 + \sigma^2 {u_2}^2\right\} - DN^2\theta_2 + CBrB_1M^2(E + u_2)^2 = 0 \tag{14}$$

Where

$$A = (1-\phi)^{2.5}\left\{(1-\phi) + \phi\frac{(\rho\beta)_s}{(\rho\beta)_f}\right\},\ P_1 = P(1-\phi)^{2.5}$$

$$B = \left(1 + \frac{3(\sigma_e - 1)\phi}{(\sigma_e + 2) - (\sigma_e - 1)\phi}\right)\frac{\sigma_f}{\sigma_e},\ B_1 = (1-\phi)^{2.5}B$$

$$C = \frac{1}{(1-\phi)^{2.5}}\left\{\frac{K_s + 2K_f + \phi(K_f - K_s)}{K_s + 2K_f - 2\phi(K_f - K_s)}\right\},\ D = (1-\phi)^{2.5}C$$

In Region-3

$$\frac{d^2u_3}{dy^2} + Gr\theta_3 + P - M^2(E + u_3) = 0 \tag{15}$$

$$\frac{d^2\theta_3}{dy^2} + Br\left(\frac{du_3}{dy}\right)^2 - N^2\theta_3 + BrM^2(E + u_3)^2 = 0 \tag{16}$$

The boundary and interface conditions become:

	Velocity	Temperature
at $y = -h$	$u_1(-1) = 0$	$\theta_1(-1) = 0$
at $y = 0$	$u_1(0) = u_2(0)$	$\theta_1(0) = \theta_2(0)$
	$\frac{du_1(0)}{dy} = \frac{\mu_{nf}}{\mu_f}\frac{du_2(0)}{dy}$	$\frac{d\theta_1(0)}{dy} = \frac{k_{nf}}{k_f}\frac{d\theta_2(0)}{dy}$
at $y = h$	$u_2(1) = u_3(1)$	$\theta_2(1) = \theta_3(1)$
	$\frac{du_2(1)}{dy} = \frac{\mu_f}{\mu_{nf}}\frac{du_3(1)}{dy}$	$\frac{d\theta_2(1)}{dy} = \frac{k_f}{k_{nf}}\frac{d\theta_3(1)}{dy}$
at $y = 2h$	$u_2(2) = 0$	$\theta_2(2) = 1$

(17)

3. Solution of the temperature & velocity field

The closed form of the result is obtained for electro-magnetic three-phase flow in a permeable channel by using the regular perturbation method by assuming the *Br* to be perturbation persistent. The dimensionless governing equations (11) to (16) which are nonlinear and coupled are solved using the boundary and interface constraints Eq. (17) for flow and heat distribution profile. This set of equations is converted using the following form:

$$u_i(y) = u_{i0}(y) + Bru_{i1} + (Br)^2 u_{i2}(y) + \ldots\ldots \tag{18}$$

$$\theta_i(y) = \theta_{i0}(y) + Br\theta_{i1} + (Br)^2\theta_{i2}(y) + \ldots\ldots \tag{19}$$

By comparing the coefficients of the similar powers of *Br* to zero we get.

a. Zeroth order equations

In Region-1

$$\frac{d^2u_{10}}{dy^2} + Gr\,\theta_{10} + P - M^2(E + u_{10}) = 0 \tag{20}$$

$$\frac{d^2\theta_{10}}{dy^2} - N^2\theta_{10} = 0 \tag{21}$$

In Region-2

$$\frac{d^2u_{20}}{dy^2}+AGr\theta_{20}-\sigma^2u_{20}+P_1-B_1M^2(E+u_{20})=0 \tag{22}$$

$$\frac{d^2\theta_{20}}{dy^2}-DN^2\theta_{20}=0 \tag{23}$$

In Region-3

$$\frac{d^2u_{30}}{dy^2}+Gr\theta_{30}+P-M^2(E+u_{30})=0 \tag{24}$$

$$\frac{d^2\theta_{30}}{dy^2}-N^2\theta_{30}=0 \tag{25}$$

The boundary and interface constraints are:

	Velocity	Temperature
at $y=-h$	$u_{10}(-1)=0$	$\theta_{10}(-1)=0$
at $y=0$	$u_{10}(0)=u_{20}(0)$	$\theta_{10}(0)=\theta_{20}(0)$
	$\frac{du_{10}(0)}{dy}=\frac{\mu_{nf}}{\mu_f}\frac{du_{20}(0)}{dy}$	$\frac{d\theta_{10}(0)}{dy}=\frac{k_{nf}}{k_f}\frac{d\theta_{20}(0)}{dy}$
at $y=h$	$u_{20}(1)=u_{30}(1)$	$\theta_{20}(1)=\theta_{30}(1)$
	$\frac{du_{20}(1)}{dy}=\frac{\mu_f}{\mu_{nf}}\frac{du_{30}(1)}{dy}$	$\frac{d\theta_{20}(1)}{dy}=\frac{k_f}{k_{nf}}\frac{d\theta_{30}(1)}{dy}$
at $y=2h$	$u_{20}(2)=0$	$\theta_{20}(2)=1$

(26)

b. First-order equation

In Region-1

$$\frac{d^2u_{11}}{dy^2}+Gr\theta_{11}-M^2u_{11}=0 \tag{27}$$

$$\frac{d^2\theta_{11}}{dy^2}+\left(\frac{du_{10}}{dy}\right)^2-N^2\theta_{11}+M^2(E+u_{10})^2=0 \tag{28}$$

In Region-2

$$\frac{d^2u_{21}}{dy^2}+AGr\theta_{21}-\sigma^2u_{21}-B_1u_{21}M^2=0 \tag{29}$$

$$\frac{d^2\theta_{21}}{dy^2}+C\left\{\left(\frac{du_{20}}{dy}\right)^2+\sigma^2u_{20}^2\right\}+B_1CM^2(E+u_{20})^2-DN^2\theta_{21}=0 \tag{30}$$

In Region-3

$$\frac{d^2u_{31}}{dy^2}+Gr\theta_{31}-M^2u_{31}=0 \tag{31}$$

$$\frac{d^2\theta_{31}}{dy^2}+\left(\frac{du_{30}}{dy}\right)^2-N^2\theta_{31}+M^2(E+u_{30})^2=0 \tag{32}$$

The boundary and interface constraints are:

	Velocity	Temperature
at $y=-h$	$u_{11}(-1)=0$	$\theta_{11}(-1)=0$
at $y=0$	$u_{11}(0)=u_{21}(0)$	$\theta_{11}(0)=\theta_{21}(0)$
	$\frac{du_{11}(0)}{dy}=\frac{\mu_{nf}}{\mu_f}\frac{du_{21}(0)}{dy}$	$\frac{d\theta_{11}(0)}{dy}=\frac{k_{nf}}{k_f}\frac{d\theta_{21}(0)}{dy}$
at $y=h$	$u_{21}(1)=u_{31}(1)$	$\theta_{21}(1)=\theta_{31}(1)$
	$\frac{du_{21}(1)}{dy}=\frac{\mu_f}{\mu_{nf}}\frac{du_{31}(1)}{dy}$	$\frac{d\theta_{21}(1)}{dy}=\frac{k_f}{k_{nf}}\frac{d\theta_{31}(1)}{dy}$
at $y=2h$	$u_{21}(2)=0$	$\theta_{21}(2)=0$

(33)

The solutions for Eqs. (20)–(26) & Eqs. (27)–(33) along with boundary conditions are obtained by simple integration.

In Region-1

$$u_1=u_{10}+Bru_{11}$$

$$u_1=c_7\cosh My+c_8\sinh My-\left(\frac{Grc_1}{N^2-M^2}\cosh Ny+\frac{Grc_2}{N^2-M^2}\sinh Ny-\frac{P}{M^2}+E\right)$$

$$+Br\left(\begin{pmatrix}b_{41}\cosh My\\+b_{42}\sinh My\end{pmatrix}-Gr\left(\begin{matrix}-\frac{\cosh[Ny]b_{11}}{M^2-N^2}\\-\frac{\sinh[Ny]b_{12}}{M^2-N^2}\end{matrix}\right)+Gr\left(\begin{matrix}\left(-4+\frac{N^2}{M^2}+\frac{N^2\cosh[2My]}{3M^2}\right)L_{76}+\left(4-\frac{N^2}{M^2}+\frac{N^2\cosh[2My]}{3M^2}\right)L_{77}+L_{165}\cosh[(M-N)y]\\+L_{166}\sinh[(M-N)y]+L_{169}\sinh[2Ny]+L_{167}\sinh[(M+N)y]+L_{168}\cosh[(M+N)y]\\+\left(\frac{3}{M^2}-\frac{\cosh[2Ny]}{M^2-4N^2}\right)L_{82}-\left(\frac{3}{M^2}+\frac{\sinh[2Ny]}{M^2-4N^2}\right)L_{84}-\left(\frac{3}{M^2}+\frac{\cosh[2Ny]}{M^2-4N^2}\right)L_{85}\\+\frac{L_{86}(L_{12}y\cosh[My]+L_{13}y\sinh[My])}{2M}+\frac{L_{87}(L_{14}\sinh[2My]+L_1\sinh[2My])}{3M^2}\\+\frac{L_{88}\left(-2N\cosh[Ny]+\left(N^2-M^2\right)y\sinh[Ny]\right)}{\left(M^2-N^2\right)^2}-\frac{L_{89}}{M^2}\end{matrix}\right)\right)$$

$$\theta_1 = \theta_{10} + Br\theta_{11}$$

$$\theta_1 = \begin{pmatrix} c_1 \cosh Ny \\ +c_2 \sinh Ny \end{pmatrix} + Br\left(\begin{pmatrix} b_{11} \cosh Ny \\ +b_{12} \sinh Ny \end{pmatrix} - \begin{pmatrix} L_{76}\left[N^2 \cosh(2My)+4M^2-N^2\right] + L_{77}\left[N^2 \cosh(2My)-4M^2+N^2\right] + L_{88}(y \sinh[Ny]) \\ +\cosh[(M-N)y]L_{78} + \sinh[My-Ny]L_{79} + \sinh[(M+N)y]L_{80} + L_{881}(y \cosh[Ny]) + L_{89} \\ +L_{81} \cosh[(M+N)y] + L_{82}(-3+\cosh[2Ny]) + L_{83} \sinh[2Ny] + L_{84}(3+\sinh[2Ny]) \\ +L_{85}(3+\cosh[2Ny]) + L_{86}(L_{12} \cosh[My] + L_{13} \sinh[My]) + L_{87}(L_{14}+L_1)\sinh[2My] \end{pmatrix} \right)$$

In Region-2

$$u_2 = u_{20} + Bru_{21}$$

$$u_2 = c_9 \cosh Ky + c_{10} \sinh Ky - \left(\frac{AGrc_3}{D1^2-K^2} \cosh D1y + \frac{AGrc_4}{D1^2-K^2} \sinh D1y - \frac{P_1}{K^2} + \frac{B_1 EM^2}{K^2} \right)$$
$$+Br\left(\begin{pmatrix} b_{51} \cosh(L_{170})y \\ +b_{52} \sinh(L_{170})y \end{pmatrix} - AGr\begin{pmatrix} L_{144} \cosh[D1y] \\ +L_{145} \sinh[D1y] \end{pmatrix} + AGr\begin{pmatrix} L_{146} + L_{147} \sinh[2D1y] + L_{148}y \sinh[D1y] + L_{149} \sinh[Ky] + L_{150} \cosh[2D1y] \\ +L_{151}y \cosh[D1y] + L_{152} \cosh[Ky] + L_{153} \sinh[2Ky] + L_{154} \cosh[2Ky] \\ +L_{155} \cosh[(D1-K)y] + L_{156} \cosh[(D1+K)y] + L_{157} \sinh[(D1-K)y] \\ +L_{158} \sinh[(D1+K)y] \end{pmatrix} \right)$$

$$\theta_2 = \theta_{20} + Br\theta_{21}$$

$$\theta_2 = \begin{pmatrix} c_3 \cosh D1y \\ +c_4 \sinh D1y \end{pmatrix} + Br\left(\begin{pmatrix} b_{21} \cosh D1y \\ +b_{22} \sinh D1y \end{pmatrix} - \begin{pmatrix} L_{90} + L_{91} \sinh[2D1y] + L_{92}y \sinh[D1y] + L_{93} \sinh[Ky] + L_{94} \cosh[2D1y] + L_{95}y \cosh[D1y] \\ +L_{96} \cosh[Ky] + L_{97} \sinh[2Ky] + L_{98} \cosh[2Ky] + L_{99} \cosh[Ky-D1y] + L_{100} \cosh[Ky+D1y] \\ +L_{101} \sinh[Ky-D1y] + L_{102} \sinh[Ky+D1y] \end{pmatrix} \right)$$

In Region-3

$$u_3 = u_{30} + Bru_{31}$$

$$u_3 = c_{11} \cosh My + c_{12} \sinh My - \left(\frac{Grc_5}{N^2-M^2} \cosh Ny + \frac{Grc_6}{N^2-M^2} \sinh Ny - \frac{P}{M^2} + E \right)$$
$$+Br\left(\begin{pmatrix} b_{61} \cosh My \\ +b_{62} \sinh My \end{pmatrix} + Gr\begin{pmatrix} \frac{\cosh[Ny]b_{31}}{M^2-N^2} \\ +\frac{\sinh[Ny]b_{32}}{M^2-N^2} \end{pmatrix} + Gr\begin{pmatrix} \left(-4+\frac{N^2}{M^2}+\frac{N^2\cosh[2My]}{3M^2}\right)L_{128} + \left(4-\frac{N^2}{M^2}+\frac{N^2\cosh[2My]}{3M^2}\right)L_{129} - \frac{L_{139}}{M^2} - \frac{\cosh[(M-N)y]L_{130}}{2MN-N^2} \\ -\frac{\sinh[(M-N)y]L_{132}}{2MN-N^2} + \frac{\sinh[(M+N)y]L_{133}}{2MN+N^2} + \frac{\cosh[(M+N)y]L_{131}}{2MN+N^2} + \frac{L_{137}\sinh[2My]}{3M^2} \\ +\left(\frac{3}{M^2}-\frac{\cosh[2Ny]}{M^2-4N^2}\right)L_{140} - \frac{\sinh[2Ny]L_{141}}{M^2-4N^2} + \left(\frac{3}{M^2}-\frac{\sinh[2Ny]}{M^2-4N^2}\right)L_{142} + \left(\frac{3}{M^2}-\frac{\cosh[2Ny]}{M^2-4N^2}\right)L_{143} \\ +\frac{L_{136}(L_{116}y \cosh[My] + L_{117}y \sinh[My])}{2M} + \frac{L_{138}\left(-2N \cosh[Ny] + \left(N^2-M^2\right)y \sinh[Ny]\right)}{\left(M^2-N^2\right)^2} \end{pmatrix} \right)$$

$$\theta_3 = \theta_{30} + Br\theta_{31}$$

$$\theta_3 = \begin{pmatrix} c_5 \cosh Ny \\ +c_6 \sinh Ny \end{pmatrix} + Br\left(\begin{pmatrix} b_{31} \cosh Ny \\ +b_{32} \sinh Ny \end{pmatrix} - \begin{pmatrix} L_{128}\left[N^2 \cosh(2My)+4M^2-N^2\right] + L_{129}\left[N^2 \cosh(2My)-4M^2+N^2\right] + \cosh[(M-N)y]L_{130} \\ +\cosh[(M+N)y]L_{131} + \sinh[(M-N)y]L_{132} + \sinh[(M+N)y]L_{133} + L_{140}(-3+\cosh[2Ny]) \\ +L_{141}\sinh[2Ny] + L_{142}(3+\sinh[2Ny]) + L_{143}(3+\cosh[2Ny]) + L_{136}(L_{116}\cosh[My] + L_{117}\sinh[My]) \\ +L_{137}\sinh[2My] + L_{138}y\sinh(Ny) + L_{1381}y\cosh(Ny) + L_{139} \end{pmatrix} \right)$$

c. Derived quantities

- **Nusselt number**

$$(Nu)_{y=-1} = \left(\frac{d\theta_1}{dy}\right)_{y=-1} \qquad (Nu)_{y=2} = -\left(\frac{d\theta_3}{dy}\right)_{y=2}$$

- **Skin friction**

$$(\tau)_{y=-1} = \left(\frac{du_1}{dy}\right)_{y=-1} \qquad (\tau)_{y=2} = -\left(\frac{du_3}{dy}\right)_{y=2}$$

4. Discussion

The velocity and heat transport behaviour multi-layer flow of electromagnetic nanofluid sandwiched between the clear fluid in the presence of thermal radiation is evaluated theoretically. The simulations are carried out by considering ethylene glycol as a base fluid and cobalt ferrite nanoparticle. For computations, the non-dimensional parameter values as $Gr = 5$, $Br = 0.1$, $P = 5$, $\sigma = 4$, $E = 1$, $N = 2$, $M = 1.5$ & $\omega = \pi/12$. Except for the modifications in the corresponding Figures and tables, these values are maintained constant throughout the study. In the following figures, the *X*-axis denoted the distance and the *Y*-axis velocity ($m \cdot s^{-2}$) or temperature (K) respectively.

In Figure 2(a)(b), we study the effects of Lorentz force on the momentum and heat transport distribution in nanofluid and clear regions. It is perceived that the momentum reaches a maximum in the clear fluid region and temperature is observed to be at the peak in the nanofluid region. It is observed from Figure 2(a)(b) that the magnetic parameter degraders the velocity and enhances the temperature profile. The observed phenomenon, known as the Hartmann effect, occurs when the applied magnetic field opposes the flow velocity. It is characterized by a ratio of electromagnetic force to viscous force. Increasing the magnetic field leads to an increase in viscosity, which in turn dampens the flow velocity and raises the temperature of the fluid.

The consequence of the electric field on the thermal distribution and velocity of fluid can be investigated in Figure 3(a)(b). Graphs are plotted for increasing values of electric field parameters in both cases. But the outcome of the variation is different in both. Velocity decreases and temperature increases with increases in the electric field. It's

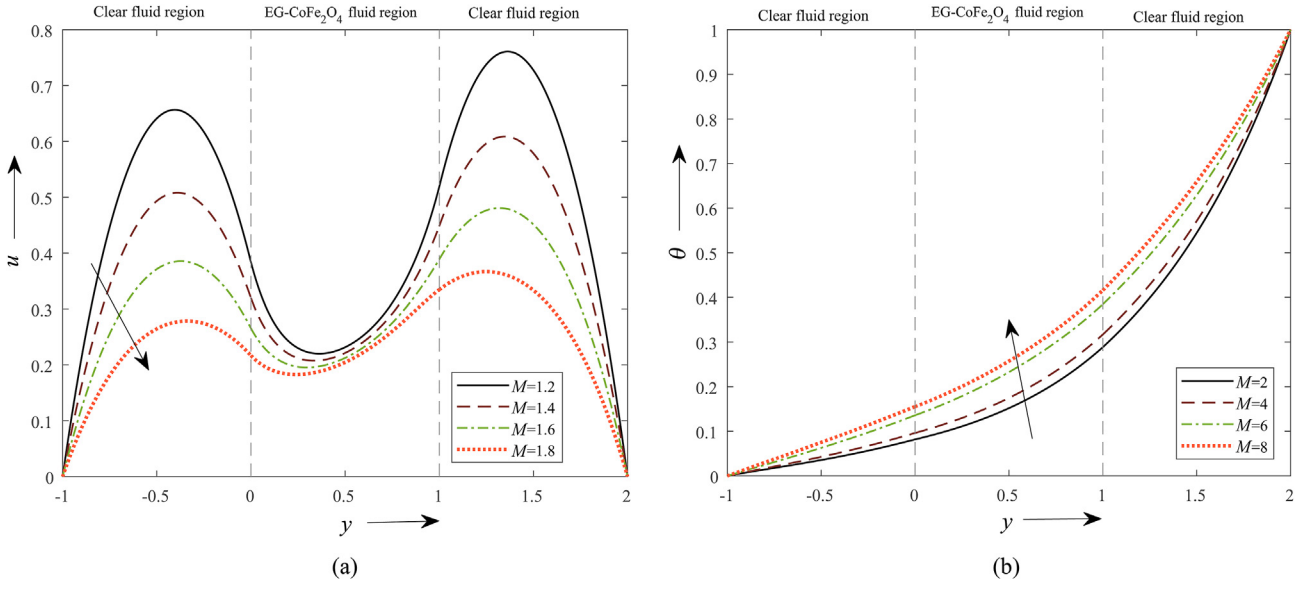

Figure 2 (a) Velocity & (b) thermal distribution across the channel with different values of *M*.

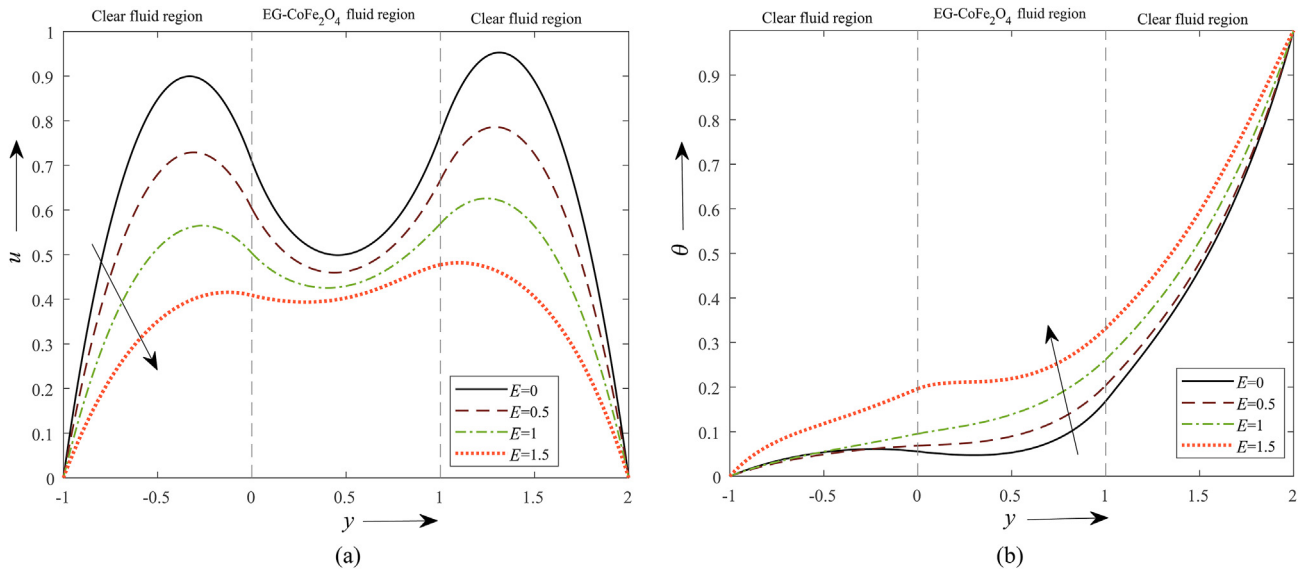

Figure 3 (a) Velocity & (b) thermal distribution across the channel with various values of E.

due to the development of the resistance in the fluid flow which clusters the molecules reduces the velocity of the fluid and increases the temperature.

Diverse values of thermal radiation on the momentum and heat transport behaviours can be seen in Figure 4(a)(b). It is observed that an increment in N, a decrease in the momentum and heat transport equations within the boundary. It follows from the reason that as the radiation parameter increases thermal conductivity decreases for all the combinations of nanofluids.

From 5(a) the effect of variation in Gr over velocity can be observed. Gr values can be increased to increase the fluid flow's momentum. The least momentum is observed in region 2 due to the porous medium and nanofluid, whereas regions 1 & 3 consist of clear fluid in the absence of a permeable medium. Thus, the distinction between the regions is apparent. Figure 5(b) shows similar results for temperature. The variation of momentum for several values of Br is shown in Figure 6(a). From the figure, it is clear that the momentum of the fluid flow increases with the increment of the Br values. The higher value is observed in region 3 followed by regions 1 & 2. The same effect is observed when temperature graphs are plotted by varying Br in Figure 6(b). The cause of this phenomenon is due to the improvement of heat produced to dissipation effects. Buoyancy force increases due to the increment of viscous dissipation, which leads to an increase in buoyancy force, hence the increment in momentum can be seen.

Figure 7(a)(b) gives a clear picture of how affects the temperature and velocity of flow. The decrease in velocity

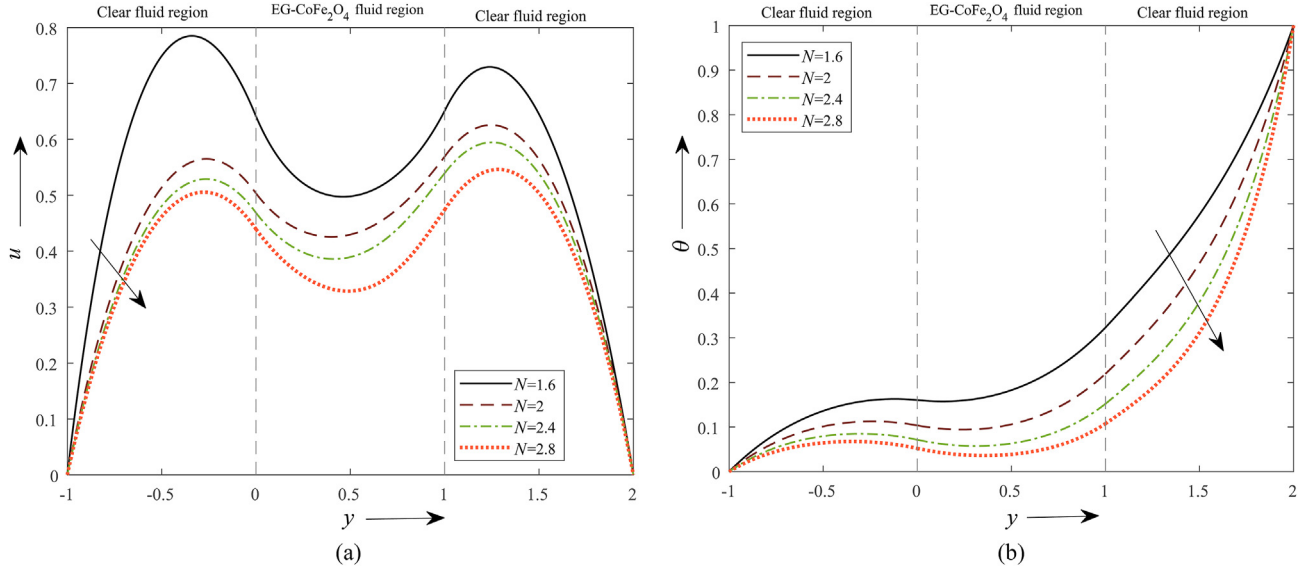

Figure 4 (a) Velocity & (b) thermal distribution across the channel with various values of N.

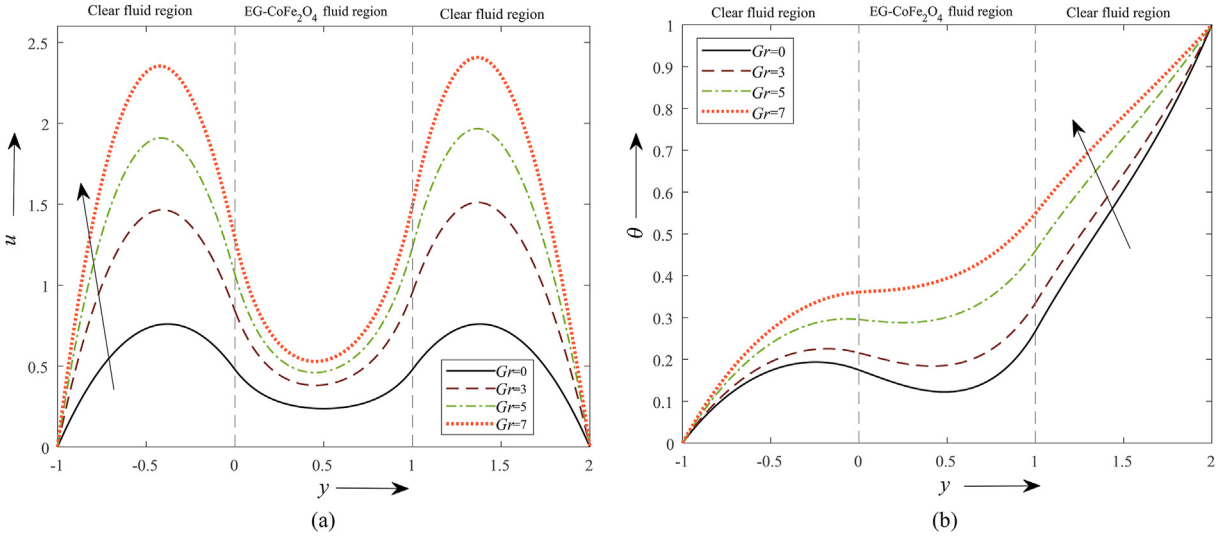

Figure 5 (a) Velocity & (b) thermal distribution across the channel with various values of *Gr*.

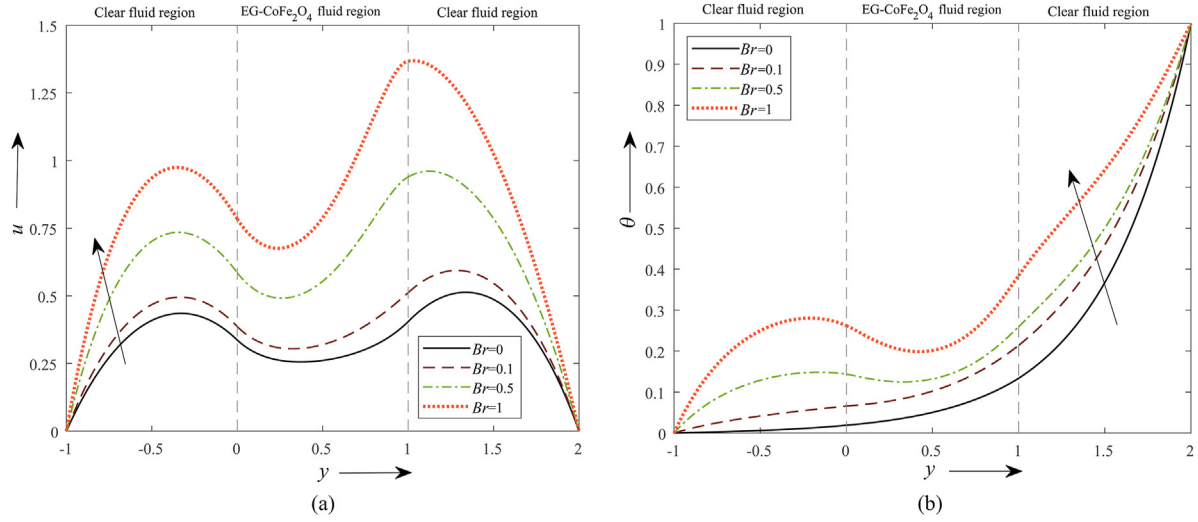

Figure 6 (a) Velocity & (b) thermal distribution across the channel with various values of *Br*.

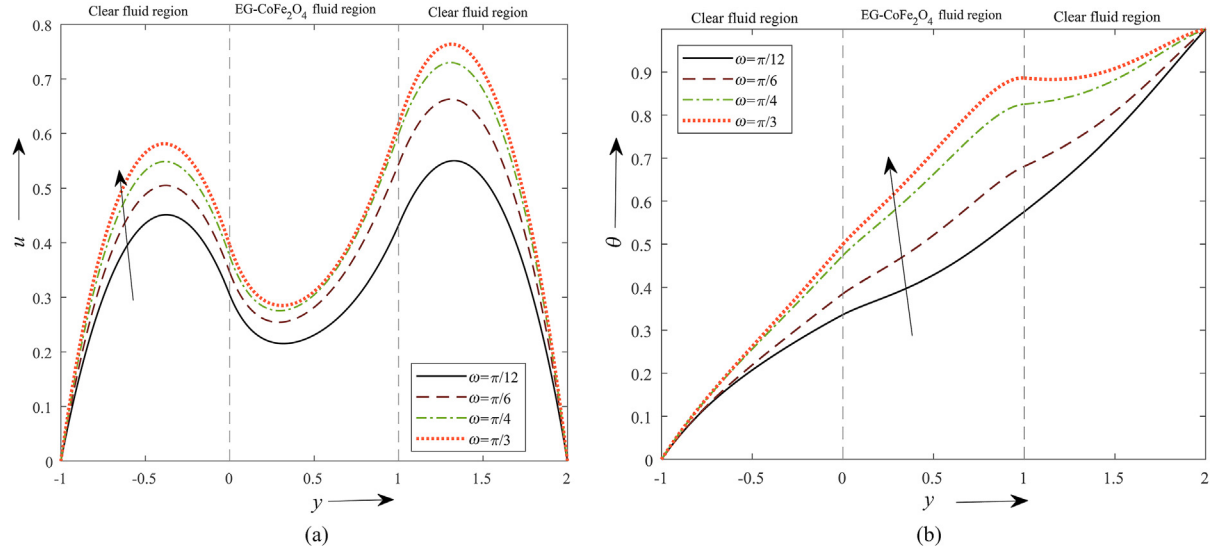

Figure 7 (a) Velocity & (b) thermal distribution across the channel with various values of ω.

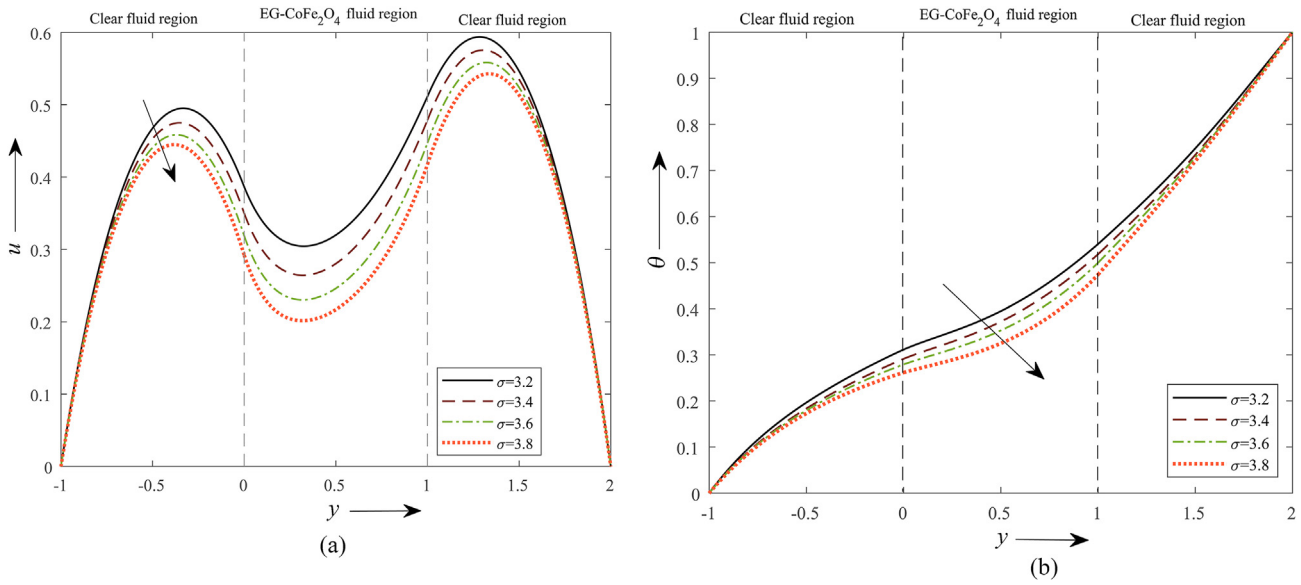

Figure 8 (a) Velocity & (b) thermal distribution across the channel with various values of σ.

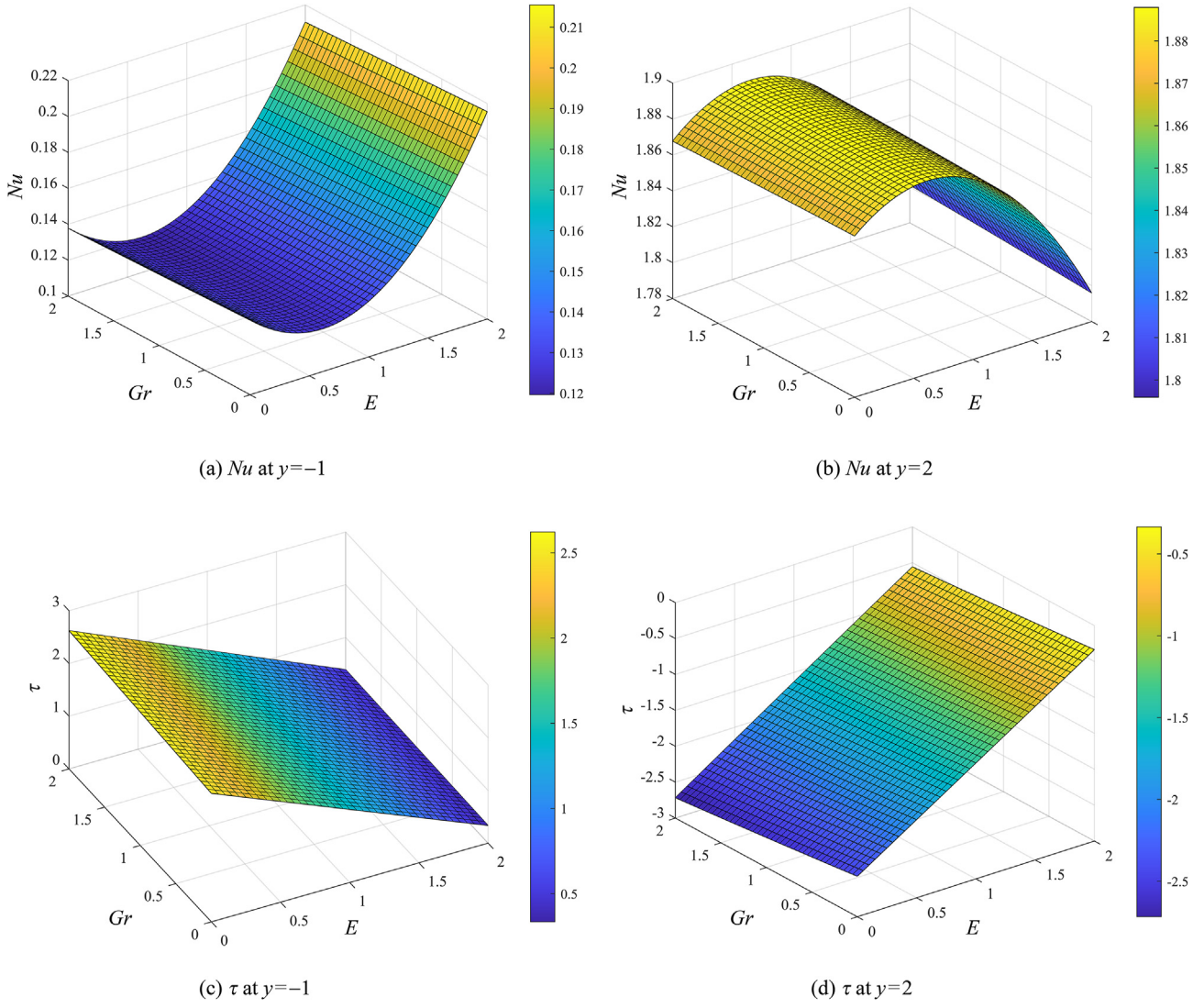

(a) *Nu* at $y=-1$

(b) *Nu* at $y=2$

(c) τ at $y=-1$

(d) τ at $y=2$

Figure 9 Graphs for variation of *Gr* and *E*.

can be observed with an increase in inclination, which is due to the upsurge of magnification of the drag force acting on the momentum. The consequence of temperature and momentum is visible in Figure 8(a)(b). Figure 8(b) shows a decrease in temperature for an increase in the values of a porous medium. The friction induced by the momentum and permeable medium causes a reduction in thermal conduction which is reflected in the decrement in the temperature of the flow. On the other hand, Figure 8(a) shows the velocity profile, with an increment in the permeability parameter, and the momentum drops in both regions. However, velocity is predominantly less in region 2 as it consists of a nanofluid with a porous medium. However, the enhancement temperature is high for water in the clear fluid region.

Figure 9(a)(b)(c)(d) displays the 3D plot of *Nu* and for various values of *Gr* & *E* at both the plates. Figure 9(a)(c) is plotted for $y = -1$ and Figure 9(b)(d) is obtained for $y = 2$. For linear increments in the values of *Gr* and *E*, an upsurge in *Nu* can be noticed. Consider Figure 9(a) & assume the *Gr* to be constant for incrementing the values of *E*, the heat transfer rate reaches maximum linearly with a positive slope, whereas at $y = 2$ decreases with incrementing the values of *E*. By altering the value of *Gr* while keeping *E* constant, the outcomes can be evaluated.

The variation of thermal radiation & magnetic field on Nusselt number and skin friction is shown in Figure 10(a)(b)(c)(d). From Figure 10(a)(b) it can be observed that *Nu* increases gradually by incrementing the values of *M* & *N*. As *Nu* increases, heat dissipation is from the fluid to the wall. Figure 10(c)(d) also gives similar results for τ. Figure 11, is a plot of *Br* & *E* for various values of *Nu* and τ at the plates. Figure 11(a) conspires for the nusselt number at $y = -1$ and Figure 11(b) at $y = 2$. It is observed that as *Br* & *E* increases, *Nu* increases exponentially. It can be inferred from this that the increase of *Nu*, transfers the heat is fluid to the wall. In Figure 11(c)(d) by keeping *Br* as a constant and incrementing the values of *E* we can notice that skin friction decreases at the right plate, whereas at $y = 2$ an increase can be noticed from negative values to positive values.

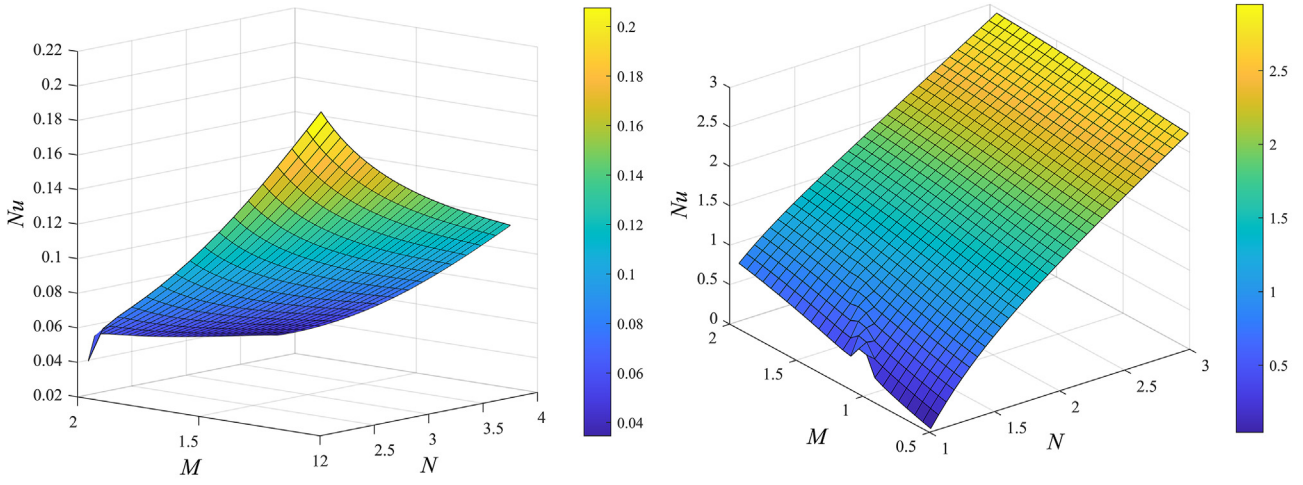

(a) *Nu* at $y=-1$ (b) *Nu* at $y=2$

(c) τ at $y=-1$ (d) τ at $y=2$

Figure 10 Graphs for variation of *N* and *M*.

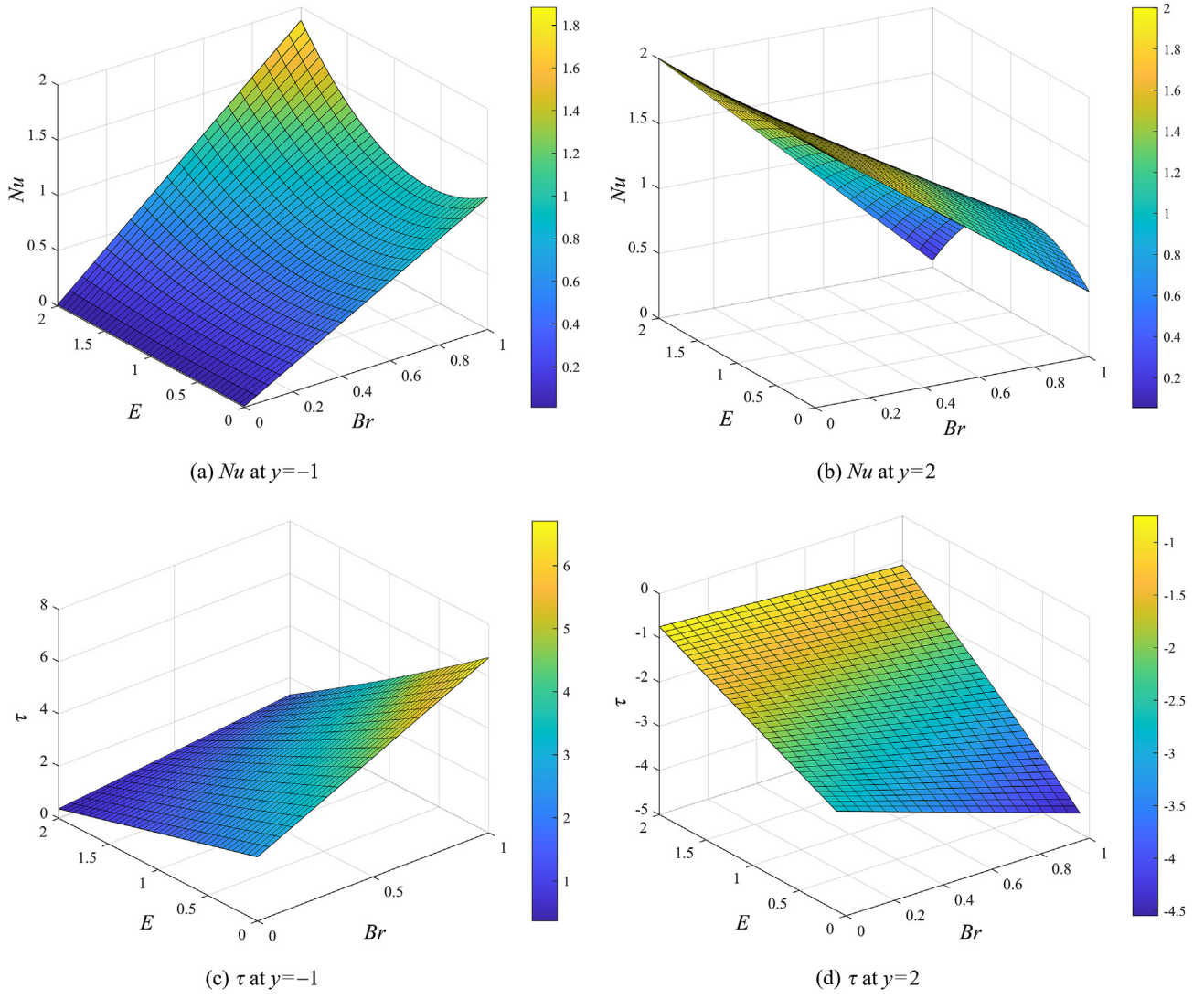

(a) Nu at $y=-1$ (b) Nu at $y=2$

(c) τ at $y=-1$ (d) τ at $y=2$

Figure 11 Graphs for variation in Br and E.

Table 3 Comparison table to the previous studies by considering $M = E = N = 0$.

y	Velocity			Temperature		
	Vajravelu et al. [41]	Umavathi et al. [34]	Present study	Vajravelu et al. [41]	Umavathi et al. [34]	Present study
−1	0	0	0	0	0	0
−0.8	4.6835	4.6835	4.6833	1.0418	1.0418	1.0417
−0.6	8.964	8.9641	8.9646	1.7608	1.7608	1.7608
−0.4	12.6966	12.6966	12.6966	2.231	2.231	2.2312
−0.2	15.7859	15.7859	15.7859	2.5206	2.5206	2.5207
0	18.1731	18.1731	18.1731	2.6897	2.6897	2.6897
0.2	19.7438	19.7438	19.7437	2.784	2.784	2.784
0.4	20.5982	20.5982	20.5982	2.8493	2.8493	2.8493
0.6	20.7236	20.7236	20.7236	2.9067	2.9067	2.9067
0.8	20.1091	20.1091	20.1090	2.9627	2.9627	2.9627
1	18.7442	18.7442	18.7442	3.0067	3.0067	3.0068
1.2	16.5095	16.5095	16.5095	3.008	3.008	3.008
1.4	13.4749	13.4749	13.4749	2.9064	2.9064	2.9064
1.6	9.6621	9.6621	9.6621	2.6186	2.6186	2.6187
1.8	5.1305	5.1305	5.1305	2.0316	2.0316	2.0316
2	0	0	0	1	1	1

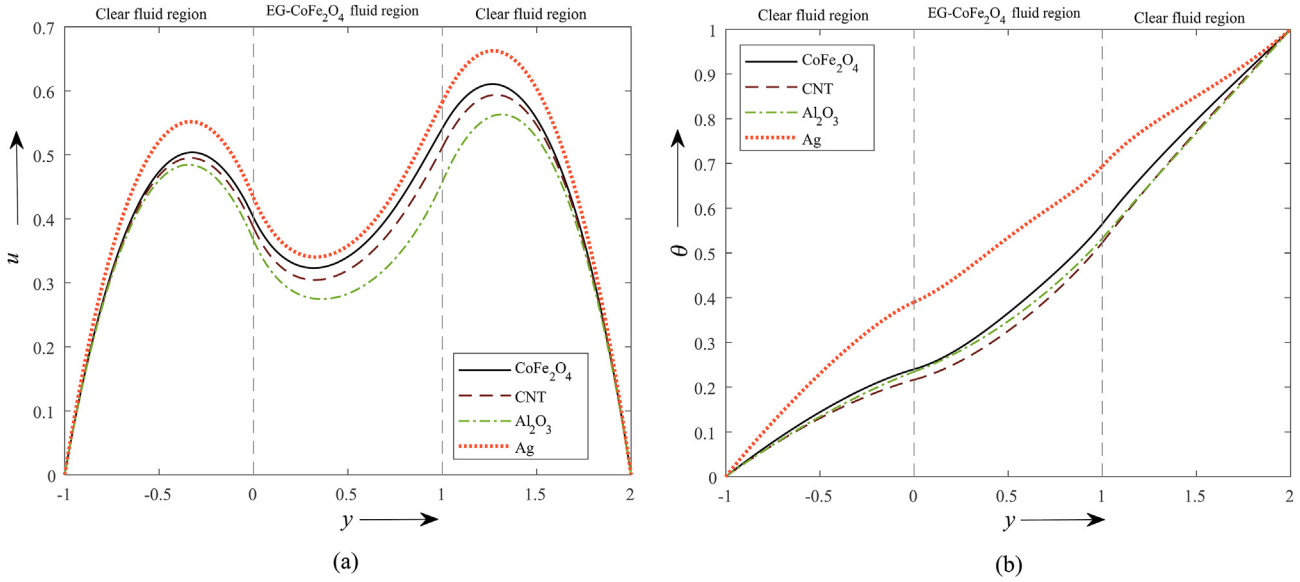

Figure 12 (a) Velocity & (b) temperature profiles for different nanoparticles.

a. Validation study

Authentication of the current study is carried out by comparing our results with two studies available in the literature (Table 3). Vajravelu et al. considered a vertical channel with three regions with finite lengths where the middle region is nanofluid and is bounded by the clear viscous fluid. Umavathi & Hemavathi studied the thermal distribution of nano-sized particles drenched with permeable medium flanked by the clear fluid in a perpendicular channel. They have considered the solid volume fraction to determine the behaviour of nanofluids. From Table 3 we conclude that our results are in good agreement with the literature, confirming the precision of the current method.

b. Comparison with different nanoparticles

Figure 12(a)(b) is the momentum and heat distribution profiles for different nanoparticles considering ethylene glycol as a solvent. The set of nanoparticles considered are used for drug delivery, these particles have a different effect which is noted from the graphs. Momentum is observed to be optimal for silver and least for Alumina nanoparticles as seen in Figure 12(a). Heat distribution is also observed to be at most for silver and minimal for carbon nanotubes (CNT) can be seen in Figure 12(b). A similar study was conducted by Umavathi and Shekhar [42], they recorded the utmost for SiO_2 and the least for Ag nanoparticles.

5. Conclusions

This study investigates the effects of radiation, magnetic, and electric fields on an incompressible steady flow of clear viscous and nanofluids in an inclined channel. The analysis focuses on understanding the impact of these fields on momentum and heat distribution. Several conclusions were drawn from this study, shedding light on the complex interactions and behaviours within the system.

- The electric & magnetic field decelerates the momentum of the flow due to the Lorentz force (electrophoretic force).
- Nusselt number and skin friction can be enhanced using the magnetic field.
- With an increase in the permeability parameter, the flow gets stronger and more symmetrical throughout the channel.
- In the clear layer, the electric field increases shear stress while decreasing it in the porous layer.
- From graphs, it is noticed that the thermal Grashof number, the angle of inclination and the Brinkman number enhance the flow and temperature of the fluids.
- The distribution of heat flux is only marginally influenced by the electric, magnetic fields and thermal radiation.
- Due to viscous dissipation, a decrease in heat transfer rate at the hot plate and an increase at the cold plot are seen.

Acknowledgements

This work was supported by the research seed grant Ref no: RU:EST:MT:2022/4 funded by REVA University and also this work was supported by the research fund of Hanyang University (HY-202300000000544).

References

[1] M.A. Maksoud, G.S. El-Sayyad, A. Ashour, A.I. El-Batal, M.S. Abd-Elmonem, H.A. Hendawy, E. Abdel-Khalek, S. Labib, E. Abdeltwab,

M. El-Okr, Synthesis and characterization of metals-substituted cobalt ferrite [MxCo(1-x) Fe2O4; (M=Zn, Cu and Mn; x=0 and 0.5)] nanoparticles as antimicrobial agents and sensors for Anagrelide determination in biological samples, Mater. Sci. Eng. C 92 (2018) 644−656, https://doi.org/10.1016/j.msec.2018.07.007.

[2] S. Sumathi, V. Lakshmipriya, Structural, magnetic, electrical and catalytic activity of copper and bismuth co-substituted cobalt ferrite nanoparticles, J. Mater. Sci. Mater. Electron. 28 (3) (2017) 2795−2802, https://doi.org/10.1007/s10854-016-5860-z.

[3] A. Al-Anazi, W.H. Abdelraheem, C. Han, M.N. Nadagouda, L. Sygellou, M.K. Arfanis, P. Falaras, V.K. Sharma, D.D. Dionysiou, Cobalt ferrite nanoparticles with controlled composition-peroxymonosulfate mediated degradation of 2-phenylbenzimidazole-5-sulfonic acid, Appl. Catal., B 221 (2018) 266−279, https://doi.org/10.1016/j.apcatb.2017.08.054.

[4] F. Falsafi, B. Hashemi, A. Mirzaei, E. Fazio, F. Neri, N. Donato, S.G. Leonardi, G. Neri, Sm-doped cobalt ferrite nanoparticles: a novel sensing material for conductometric hydrogen leak sensor, Ceram. Int. 43 (2017) 11029−11037, https://doi.org/10.1016/j.ceramint.2016.10.035.

[5] T. Dippong, O. Cadar, E.A. Levei, C. Leostean, L. Barbu Tudoran, Effect of annealing on the structure and magnetic properties of $CoFe_2O_4$:SiO_2 nanocomposites, Ceram. Int. 43 12 (2017) 9145−9152, https://doi.org/10.1016/j.ceramint.2017.04.063.

[6] C. Dey, K. Baishya, A. Ghosh, M.M. Goswami, A. Ghosh, K. Mandal, Improvement of drug delivery by hyperthermia treatment using magnetic cubic cobalt ferrite nanoparticles, J. Magn. Magn Mater. 427 (2017) 168−174, https://doi.org/10.1016/j.jmmm.2016.11.024.

[7] H. Fan, X. Xing, Y. Yang, B. Li, C. Wang, D. Qiu, Triple function nanocomposites of porous silica-$CoFe_2O_4$-MWCNTs as a carrier for pH-sensitive anti-cancer drug-controlled delivery, Dalton Trans. 46 (43) (2017) 14831−14838, https://doi.org/10.1039/C7DT02424J.

[8] K. Vamvakidis, S. Mourdikoudis, A. Makridis, E. Paulidou, M. Angelakeris, C. Dendrinou-Samara, Magnetic hyperthermia efficiency and MRI contrast sensitivity of colloidal soft/hard ferrite nanoclusters, J. Colloid Interface Sci. 511 (2018) 101−109, https://doi.org/10.1016/j.jcis.2017.10.001.

[9] S. Lee, S.U.S. Choi, S. Li, J.A. Eastman, Measuring thermal conductivity of fluids containing oxide nanoparticles, J. Heat Tran. 121 (2) (1999) 280−289, https://doi.org/10.1115/1.2825978.

[10] N.H. Hai, N.D. Phu, N.H. Luong, N. Chau, Mechanism for sustainable magnetic nanoparticles under ambient conditions, J. Kor. Phys. Soc. 52 (5) (2008) 1327−1331, https://doi.org/10.3938/jkps.52.1327.

[11] S.D. Farahani, M. Alibeigi, A. Zakinia, M. Goodarzi, The effect of microchannel-porous media and nanofluid on temperature and performance of CPV system, J. Therm. Anal. Calorim. 147 (14) (2022) 7945−7960, https://doi.org/10.1007/s10973-021-11087-5.

[12] W.K. Usafzai, E.H. Aly, A.S. Alshomrani, M.Z. Ullah, Multiple solutions for nanofluids flow and heat transfer in porous medium with velocity slip and temperature jump, Int. Commun. Heat Mass Tran. 131 (2022) 105831, https://doi.org/10.1016/j.icheatmasstransfer.2021.105831.

[13] M. Habibishandiz, M.Z. Saghir, A critical review of heat transfer enhancement methods in the presence of porous media, nanofluids, and microorganisms, Therm. Sci. Eng. Prog. 30 (2022) 101267, https://doi.org/10.1016/j.tsep.2022.101267.

[14] A. Hibara, M. Tokeshi, K. Uchiyama, H. Hisamoto, T. Kitamori, Integrated multilayer flow system on a microchip, Anal. Sci. 17 (2001) 89−93, https://doi.org/10.2116/analsci.17.89.

[15] A.R.A. Khaled, Heat transfer enhancement in a vertical tube confining two immiscible falling co-flows, Int. J. Therm. Sci. 85 (2014) 138−150, https://doi.org/10.1016/j.ijthermalsci.2014.06.023.

[16] J.C. Umavathi, O. Anwar Bég, Effects of thermophysical properties on heat transfer at the interface of two immiscible fluids in a vertical duct: numerical study, Int. J. Heat Mass Tran. 154 (2020) 119613, https://doi.org/10.1016/j.ijheatmasstransfer.2020.119613.

[17] X. Chen, Y. Jian, Entropy generation minimization analysis of two immiscible fluids, Int. J. Therm. Sci. 171 (2022), https://doi.org/10.1016/j.ijthermalsci.2021.107210.

[18] M.S. Malashetty, J.C. Umavathi, J.P. Kumar, Magnetoconvection of two-immiscible fluids in vertical enclosure, Heat Mass Tran. 42 (2006) 977−993, https://doi.org/10.1007/s00231-005-0062-x.

[19] A.J. Chamkha, Flow of two-immiscible fluids in porous and nonporous channels, 2000, Available: http://fluidsengineering.asmedigitalcollection.asme.org/.

[20] M. Sheikholeslami, M. Hatami, G. Domairry, Numerical simulation of two phase unsteady nanofluid flow and heat transfer between parallel plates in presence of time dependent magnetic field, J. Taiwan Inst. Chem. Eng. 46 (2015) 43−50, https://doi.org/10.1016/j.jtice.2014.09.025.

[21] P.V. Ananth Subray, B.N. Hanumagowda, S.V. K Varma, C.S.K. Raju, I. Khan, P. Rana, Thermo-diffusion impact on immiscible flow characteristics of convectively heated vertical two-layered Baffle saturated porous channels in a suspension of nanoparticles: an analytical study, Appl. Math. Mech.-Engl 44 (2023) 307−324, https://doi.org/10.1007/s10483-023-2956-6.

[22] O.A. Bég, A. Zaman, N. Ali, S.A. Gaffar, E.T. Bég, Numerical computation of nonlinear oscillatory two-immiscible magnetohydrodynamic flow in dual porous media system: FTCS and FEM study, Heat Tran. Asian Res. 48 (2019) 1245−1263, https://doi.org/10.1002/htj.21429.

[23] A.R.A. Khaled, K. Vafai, Heat transfer enhancement by layering of two immiscible co-flows, Int. J. Heat Mass Tran. 68 (2014) 299−309, https://doi.org/10.1016/j.ijheatmasstransfer.2013.09.040.

[24] A.K. Alzahrani, Z. Abbas, M.Z. Ullah, Chemically reactive two-phase flow of viscous-Casson fluids in a rotating channel, Alex. Eng. J. 62 (2023) 403−413, https://doi.org/10.1016/j.aej.2022.07.036.

[25] J.C. Umavathi, J.P. Kumar, A.J. Chamkha, Flow and heat transfer of a micropolar fluid sandwiched between viscous fluid layers, Rev. Can. Phys. 86 (8) (2008) 961−973, https://doi.org/10.1139/p08-022.

[26] J.C. Umavathi, M. Sheremet, Flow and heat transfer of couple stress nanofluid sandwiched between viscous fluids, Int. J. Numer. Methods Heat Fluid Flow 29 (11) (2019) 4262−4276, https://doi.org/10.1108/HFF-12-2018-0715.

[27] J. Hasnain, N. Abid, M.O. Alansari, M. Zaka Ullah, Analysis on Cattaneo-Christov heat flux in three-phase oscillatory flow of non-Newtonian fluid through porous zone bounded by hybrid nanofluids, Case Stud. Therm. Eng. 35 (2022) 102074, https://doi.org/10.1016/j.csite.2022.102074.

[28] J.K. Moses, D.P. Yusuf, C. Onwubuoya, Unsteady MHD free convective three phase flow through porous medium sandwiched between viscous fluids, Int. J. Sys. Sci. Appl. Math. 1 (4) (2016) 91−108.

[29] J.C. Umavathi, A.J. Chamkha, M.H. Manjula, A. Al-Mudhaf, Flow and heat transfer of a couple-stress fluid sandwiched between viscous fluid layers, Can. J. Phys. 83 (7) (2005) 705−720, https://doi.org/10.1139/p05-032.

[30] D. Nikodijevic, Z. Stamenkovic, M. Jovanovic, M. Kocic, J. Nikodijevic, Flow and heat transfer of three immiscible fluids in the presence of uniform magnetic field, Therm. Sci. 18 (3) (2014) 1019−1028, https://doi.org/10.2298/TSCI1403019N.

[31] A. Rauf, M. Naz, Simultaneous flow of three immiscible fractional maxwell fluids with the clear and homogeneous porous cylindrical domain 6 (2020) 1324−1334.

[32] T.N. Tanuja, L. Kavitha, S.V.K. Varma, U. Khan, E.-S.M. Sherif, A.M. Hassan, I. Pop, K. Sarada, H.S. Gill, Flow and heat transfer analysis on micropolar fluid through a porous medium between a clear and Al_2O_3-Cu/H_2O in conducting field, Front. Mater 10 (2023) 1216757, https://doi.org/10.3389/fmats.2023.1216757.

[33] P. Kumar Yadav, S. Jaiswal, T. Asim, R. Mishra, Influence of a magnetic field on the flow of a micropolar fluid sandwiched between two Newtonian fluid layers through a porous medium, The European Physical Journal Plus 133 (7) (2018) 247, https://doi.org/10.1140/epjp/i2018-12071-5.

[34] J.C. Umavathi, K. Hemavathi, Flow and heat transfer of composite porous medium saturated with nanofluid, Propuls. Power Res. 8 (2) (2019) 173−181, https://doi.org/10.1016/j.jppr.2019.01.010.

[35] D. J Tritton, Physical Fluid Dynamics, Van Nostrand Reinhold Co, New York, 1977.

[36] R.K. Tiwari, M.K. Das, Heat transfer augmentation in a two-sided lid-driven differentially heated square cavity utilizing nanofluids, Int. J. Heat Mass Tran. 50 (2007) 2002−2018, https://doi.org/10.1016/j.ijheatmasstransfer.2006.09.034.

[37] H. Darcy, Les fontaines publiques de la ville de Dijon, Dalmont, Paris, 1856.

[38] B. Kharat Prashant, S. Kounsalye Jitendra, V. Shisode, K.M. Jadhav Mahendra, Preparation and thermophysical investigations of $CoFe_2O_4$-based nanofluid: a potential heat transfer agent, J. Supercond. Nov. Magnetism 32 (2) (2019), https://doi.org/10.1007/s10948-018-4711-y.

[39] M. Devarajan, N. Parasumanna Krishnamurthy, M. Balasubramanian, B. Ramani, S. Wongwises, K. Abd El-Naby, R. Sathyamurthy, Thermophysical properties of CNT and CNT/Al_2O_3 hybrid nanofluid, Micro & Nano Lett. 13 (2018) 617−621, https://doi.org/10.1049/mnl.2017.0029.

[40] J. Maxwell, A Treatise on Electricity and Magnetism, second ed., Oxford University Press, Cambridge, UK, 1904.

[41] K. Vajravelu, K.V. Prasad, S. Abbasbandy, Convective transport of nanoparticles in multi-layer fluid flow, Appl. Math. Mech. 34 (2) (2013) 177−188, https://doi.org/10.1007/s10483-013-1662-6.

[42] J.C. Umavathi, M. Shekar, Effect of MHD on Jeffery-Hamel flow in nanofluids by differential transform method, [Online] Available: www.ijera.com.